

Role of particle/particle collisions in a dilute tube flow : Analysis and experiments for mono and bi-dispersed situations.

by

N. CARAMAN ^{****}, J. BORÉE ^{*}, I. FLOUR ^{**}

J. Borée (jacques.boree@lea.ensma.fr) is the corresponding author.

^{*} LEA ENSMA – Téléport 2 – 1, Av. Clément Ader – BP 40109
86961 FUTUROSCOPE CHASSENEUIL Cedex - FRANCE

^{**} EDF - R&D - MFTT, 6, Quai Watier , 78400 CHATOU, France

^{***} Institut de Mécanique des Fluides ; UMR CNRS/INPT-UPS 5502
Allée du Professeur Camille Soula ; 31400 TOULOUSE ; France

ABSTRACT

The present paper present measurements and analysis of a bidispersed two-phase flow at low (11%) and moderate (110%) mass loading in a fully developed pipe flow. Our goal is to provide data and analysis showing unambiguously the role of inter-class collisions. The mass distribution of the mixture of particles is therefore chosen in order to promote the collisions of the large 90 μm particles with 60 μm glass beads.

Velocity statistical moments up to the third order moments and at both mass loadings are presented and discussed. At low mass loading, it is interesting to note that the radial characteristics of the air and 60 μm glass beads for a monodispersed (Caraman et al. 2003) and a bidispersed situations (present results) are very similar. Moreover, the radial turbulent transport of longitudinal and radial fluctuating kinetic stresses is much higher for the particles than for the fluid phase. Dominant effects in the flow are then (i) in the core flow a source through the interaction with the fluid turbulence, a dissipation due to the fluid drag and a transport by the third order velocity correlation.; (ii) in the near wall region a production by the mean shear for u_p' and a redistribution from the very large streamwise velocity variance via particle-particle collisions for v_p' .

The signature of inter-particle collisions is very clear at higher mass loading. In particular, we measure a decrease of the streamwise kinetic stress of the larger particles all over the section of the tube. On the contrary, the streamwise kinetic stress of 60 μm particles decrease in the high shear region only while a slight increase of u_{p60}' is detected in the core flow. The striking result is the strong increase of the radial fluctuating velocities of the glass beads and of the radial transport of the radial fluctuating kinetic energy for $M_j = 110\%$. An analysis of the collision frequency in different regions of the flow shows that, even at $M_j = 110\%$, the mean time scale between collisions is of the order or larger than the particle aerodynamic time constant. The picture at the higher mass loading studied here is thus an important contribution of inter-particle collisions to the radial variance v_p' in the near wall region associated to a damping of the longitudinal kinetic stress. This damping is more important for 90 μm glass beads than for 60 μm glass beads because 60 μm particles receive kinetic energy from 90 μm particles. However, collisions are not able to decrease significantly the mean free path of the particle fluctuating motion. Therefore, transport effects of both longitudinal and radial fluctuating kinetic stresses toward the core region are very high and normalised pdf are quite similar at $M_j = 110\%$ and $M_j = 11\%$. The present study shows that accurate models describing the full particle kinetic stresses and the exchanges due to the collisional terms are very important for the accurate prediction of gas-solid polydispersed tube flows.

Caraman, N., Borée, J. and Simonin, O. (2003). Effect of collisions on the dispersed phase turbulence in a dilute tube flow. Experimental and Theoretical analysis. Physics of Fluids 15, (12).

1. INTRODUCTION

Wall bounded flows in rectangular channels or circular tubes form a particularly important class of single or two-phase turbulent flows. Good engineering models have to take into account a lot of inter-dependant effects and their development is therefore challenging.

For turbulent flow fields in tubes or channels laden with small particles much heavier than the gas phase, the numerical studies of (Simonin, Wang and Squire 1997; Yamamoto *et al.* 2001) have shown that particle-particle collisions in the near wall region provide a very important contribution to the radial fluctuation and therefore to the radial distribution of the particles throughout the tube even for very dilute conditions - solid volume fraction $O(10^{-4})$. The recent experimental study of (Caraman, Borée and Simonin 2003) has confirmed these statements and has proved experimentally that the collisional redistribution from the very large streamwise velocity variance to the radial velocity variance in the near wall region strongly influences the radial fluctuation of the particles and partly drives the radial transport of the fluctuating kinetic energy of the particles. Note that the behaviour of spherical solid particles in a narrow horizontal channel flow was analysed by (Sommerfeld 2003), (Kussin and Sommerfeld 2002). The effect of wall collisions are emphasised in this situation. However, a detailed analysis presented in (Caraman *et al.* 2003) show that it is not the case in the vertical tube flow discussed here.

The present paper is devoted to the experimental analysis of bi-dispersed situations in a dilute tube flow. A mixture of particles at low (11%) and moderate (110%) global mass loading will be considered. The mixture is a mixture of $60\mu\text{m}$ particles and of larger glass beads ($d_p=90\mu\text{m}$). By computing the respective probabilities of 60/60; 90/90; 60/90 and 90/60 collisions (Gourdel, Simonin and Brunier 1998), we have chosen the final distribution in order to promote the collisions of large particles with $60\mu\text{m}$ glass beads. Our goal is here mainly to provide data and analysis showing unambiguously the effects of inter-class collisions. Indeed, if collisions are important, the mean and fluctuating characteristics of different size classes are coupled because particle exchange momentum with one another. We will therefore focus on the properties of one particle size class ($60\mu\text{m}$) in relation with models devoted to binary mixtures of particles (Gourdel *et al.* 1998).

We will compare the statistical moments of the bidispersed situation with the results discussed by (Caraman *et al.* 2003) obtained with a narrow distribution of partly responsive glass beads ($d_p=60\mu\text{m}$) at a low global mass loading of 11%. The experimental set-up and measurement techniques are described in section II. Glass beads are described and selected in section III. The results and physical analysis are proposed next.

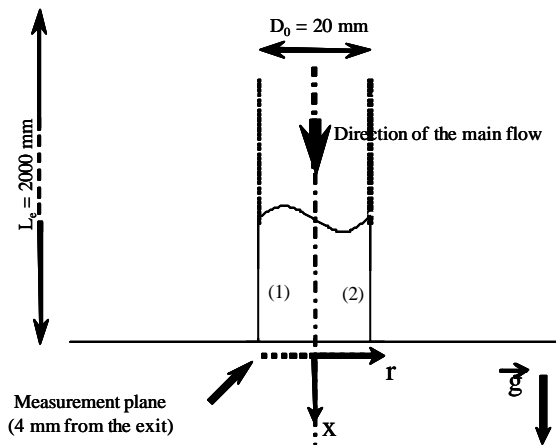


Fig. 1. Sketch of the set up.

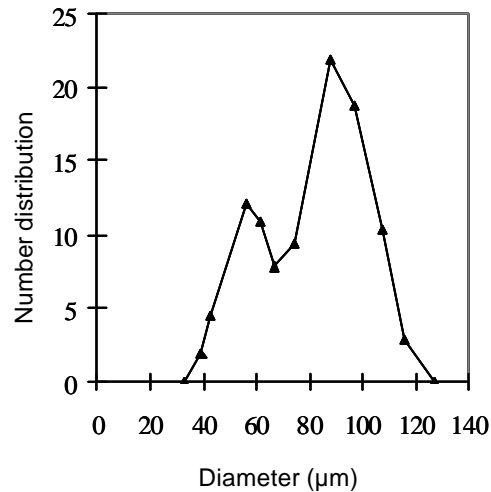


Fig. 2. Number distribution of the glass beads.

2. EXPERIMENTAL SET-UP ; MEASUREMENT TECHNIQUE

The present data are obtained at the exit of a tube (figure 1). The material of the tube is A-G type aluminium. The tube flow ($D_0 = 2R_0 = 20mm$) is generated by compressed air. The volume flux of the jet is $Q_j = 3.4 m^3/h$. This corresponds to a bulk velocity $\overline{U}_j = 3.4 m/s$ and a velocity on the axis $\langle U \rangle_f (r=0) = 4 m/s$ in single phase flow or at low mass loading. The length of the tube is $L_e = 2m$. The single phase flow is therefore established with $L_e/R_0 = 200$. The Reynolds number $Re_0 = U_0 D_0 / \nu \approx 5300$ - ν is the kinematic viscosity of air - is fairly low but extensive tests have shown that the single phase flow is fully turbulent. The friction velocity u^* of the single-phase pipe flow evaluated from the slope of the Reynolds shear stress profile at the channel centre (Caraman *et al.* 2003) is $u^* = 0.2 \pm 0.01 m/s$. The Reynolds number based on u^* is thus $Re_t = u^* R_0 / \nu \approx 133$. Figure 1 shows that measurements are obtained $x = 4 mm$ (i.e. $x/D_0 = 0.2$) downstream the exit of the tube. Measurements closer to the exit are not possible with the present set-up. The time needed to travel the distance $0.2D_0$ at the mean velocity U_0 ($t \approx 1 ms$) is much smaller than the integral time scale of the turbulence in the core flow. At the measurement location, the core flow still carries all the properties of the tube turbulence.

A two components phase Doppler anemometer produced by Dantec (Particle Dynamics Analyser: PDA) is used. Total intersection angle of incident beam is 1.5 degree. The receiving optics is settled at 64 degrees of off-axis angle from the incident beam to minimise the contribution of the reflected light - (Borée, Ishima and Flour 2001). The used refractive index is set as 1.51 and corresponds to normal glass particle. Smoke was used to generate the tracer particles. Their refractive indexes are not equal to that of glass particles. However, the result from the single phase flow measurements with only seeding particles but performed with the refractive index of the glass particle indicates that the mean diameter of smoke is $2\mu m$. In addition, the results from two-phase flow without tracers show that very few glass particles with less than $10 \mu m$ in diameter exist in the experimental region. Therefore, all the particles with less than $5 \mu m$ in diameter are treated as tracer particles. We have verified that all the particles in this size-class can be considered as good tracers of the continuous phase. Their Stokes number based on the Kolmogorov time scale is indeed lower than 0.1 everywhere in the flow. At low mass loading (11%), measurements are carried out for the continuous and dispersed phases simultaneously. At higher mass loading (110%), measurements are only carried out for the dispersed phase. Indeed, any attempt to obtain simultaneously tracers and glass beads data at this loading leads to very noisy data because the photomultiplier high voltage was set at a high level.

All the statistics presented in the paper are computed from at least 10.000 independent samples in the continuous phase and in the size-class. Consequently, estimated statistical absolute errors for mean values are respectively - (Benedict and Gould 1996)- $\Delta \langle U \rangle \approx 0.02u'$, $\Delta u' \approx 1.4 \cdot 10^{-2} u'$, $\Delta \langle uv \rangle \approx 0.03u' v'$, $\Delta \langle uuu \rangle \approx 0.05u'^3$ and $\Delta \langle uuv \rangle \approx 0.05 u'^2 v'$ with a 95% confidence level.

The flow will be described henceforth using a cylindrical co-ordinate system (x,r,θ) to indicate the axial (downward), radial and azimuthal directions. The origin is set on the axis of the tube in the measurement section. The components of the instantaneous velocity field are denoted respectively by (U,V,W) where V is the radial component and W is the azimuthal component. No mean swirling motion was detected to within our measurement precision. Subscripts “f” and “p” indicate fluid and particles properties respectively. The symbol $\langle \rangle_f$ and $\langle \rangle_p$ indicates averaging operators associated respectively to fluid and particle phases. The components of the instantaneous fluctuating velocity field are denoted respectively by (u,v,w) . The expressions u' and v' stand respectively for longitudinal and radial standard deviation.

3 SELECTION OF PARTICLE DISTRIBUTION

Glass particles (density $\rho_p = 2470 kg/m^3$) are released in the conducting pipe by a particle feeder. All parts of the set-up were carefully grounded and the air flow is slightly humid in order to suppress the influence of electrostatics. All flow conditions and particle mass loading are monitored on a PC. The mass loading is controlled accurately in closed loop by

weighting continuously the particle feeder. Mass fluxes of particles of 0.5 kg/h and 5 kg/h corresponding respectively to mass loading ratio $M_j = 11\%$ and 110% have been selected.

The particles were new at the beginning of this work. The distribution was checked several times during the acquisition of the data base in order to check for possible breaking of particles during runs. No noticeable differences were detected. Moreover, visual inspection with a microscope revealed very few non-spherical glass fragments. The number distributions of the size of the spherical glass beads is presented in figure 2. The width of the size classes is $10 \mu\text{m}$. Note that all the measurements for “60 μm ” particles will be based on samples belonging to the size-class $55 \mu\text{m} \leq d_p \leq 65 \mu\text{m}$.

The bidispersed size distribution of figure 2 was obtained by mixing two narrow dispersions respectively centred on 60 μm and 90 μm . The proportion of large glass beads was chosen in order to promote inter-class collisions. In a first guess, let’s suppose that the mean and fluctuating velocities of classes “i” and “j” are equal. It is straightforward to show by using the relation (5.1) presented in section 5 that:

$$\frac{f_{Ci,j}}{f_{Ci,i}} = \frac{n_j}{4n_i} \left(1 + \frac{r_{pj}}{r_{pi}}\right)^2 ; \frac{f_{Cj,j}}{f_{Cj,i}} = \frac{n_j}{n_i} \left(\frac{r_{pj}}{r_{pi}}\right)^2$$

$f_{Ci,j}$ is the mean frequency of collision between a particle of size class “i” and the class “j”; r_p is the radius of the particle, n_j is the number concentration for class j. The final bidispersed mixture was obtained by mixing 13% in mass of 60 μm dispersion and 87% in mass of 90 μm dispersion. The ratio of mass and number concentrations are then respectively $m_{90}/m_{60} = 6,7$ and $n_{90}/n_{60} = 2$. The following approximate relations then hold: $f_{C60,90} \approx 3.1 f_{C60,60}$ and $f_{C90,60} \approx 0.3 f_{C90,90}$. We see that, if collisions are important, the inter-class effects will dominate in the 60 μm class while in-class effects will dominate in the 90 μm class.

A detailed analysis presented in (Caraman et al. 2003) and not repeated here shows that the 60 μm glass beads (and obviously 90 μm ones) don’t respond to the local turbulent scales in the near wall region. On the axis of the pipe, 60 μm particles (resp. 90 μm) correspond to a Stokes number $S_t = \tau_p/\tau_t$ of order 3 (resp. of order 7). τ_p is the particle aerodynamic time scale; τ_t is the turbulent integral time scale.

4 RADIAL EVOLUTIONS OF STATISTICAL MOMENTS

The streamwise mean velocity of air, 60 μm particles and 90 μm particles respectively are drawn in figure 3. All the radial evolutions presented in this paper will be displayed in the same way: the air characteristics have been measured at the lowest mass-loading only. The whole air data profile is therefore presented for $M_j = 11\%$. The right hand side (resp. left hand side) of the figures is devoted to 60 μm glass beads (resp. 90 μm glass beads) ; black symbols correspond to low mass loading while grey symbol correspond to high mass loading.

The figure 3 shows that the mean velocity of the particles becomes increasingly larger than the fluid velocity in the region of maximum mean shear near the wall. This effect due to inertia is a maximum for the larger size classes. For example, at $r=9\text{mm}$ and $M_j = 11\%$, $\langle U_f \rangle_f = 2.56 \text{ m/s}$; $\langle U_p \rangle_{p60} = 3.10 \text{ m/s}$ and $\langle U_p \rangle_{p90} = 3.35 \text{ m/s}$. The figure 3 also shows clearly that the mean velocity profile of the particulate phase is flatter at $M_j = 110\%$ with a lower value of the mean velocity of the glass beads on the axis. In a tube flow, the role of the radial turbulent transport of the longitudinal fluctuating particle velocity is clearly to decrease $\langle U_p \rangle_p$ in the core region – see for example (Caraman et al. 2003). The figure 4 shows that this transport is higher at $M_j = 110\%$. A more uniform mean velocity profile of the glass beads at the higher loading is therefore expected. Note also that the mass flux of air is the same for both situations and corresponds to a bulk velocity $\bar{U}_j = 3.4 \text{ m/s}$. The velocity of air was unfortunately not measured at $M_j = 110\%$ but we expect that two-way coupling is responsible for a flatter air velocity profile and, as a consequence for a lower value of the air velocity on the axis at the higher loading.

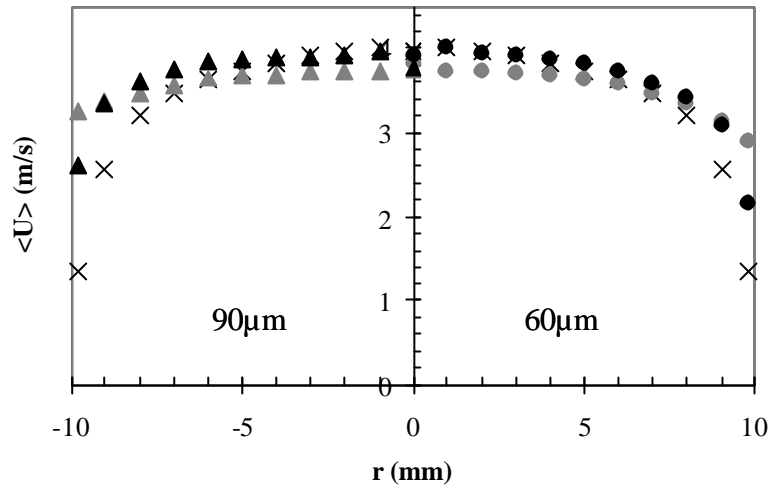


Fig. 3. Mean velocity profile. X, Tracers;
 Right side. $d_p = 60\mu\text{m}$? , $M_j = 11\%$; ? , $M_j = 110\%$;
 Left side. $d_p = 90\mu\text{m}$? , $M_j = 11\%$; ? , $M_j = 110\%$.

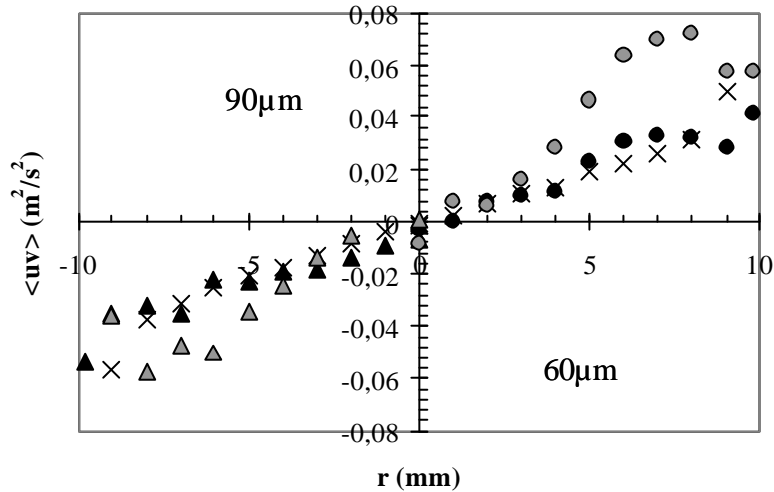


Fig. 4. Reynolds shear stress. (Symbols : see fig 3)

At low mass loading, we see in figure 5 that the axial fluctuation intensities of both $60\mu\text{m}$ and $90\mu\text{m}$ size classes are larger than the air turbulence intensity in the streamwise direction. The difference is very important in the core flow. Moreover, the radial kinetic stress of these large particles is very similar to v_f' . Radial balance of longitudinal and radial kinetic stresses were analysed in detail in this tube flow (Caraman et al. 2003) for a monodispersed size distribution of $60\mu\text{m}$ particles at $M_j = 11\%$ only. In agreement with the numerical studies of (Simonin et al. 1997) and (Yamamoto et al. 2001), we found in this previous study that the dominant effects are : (i) in the core flow a source through the interaction with the fluid turbulence, a dissipation due to the fluid drag and a transport by the third order velocity correlation ; (ii) in the near wall region a production by the mean shear for u_p' and a redistribution from the very large streamwise velocity variance via particle-particle collisions for v_p' . An important result of this previous study was that the radial turbulent transport of longitudinal and radial fluctuating kinetic stresses is much higher for the particles than for the fluid phase. We will come back to this point.

At low mass loading, it is interesting to note that the radial characteristics of the air and 60 μm glass beads for a monodispersed (Caraman et al. 2003) and a bidispersed situations (present results) are very similar. An increase of the mass loading obviously induces very strong variations detected in figure 5. In particular, we measure a decrease of the streamwise kinetic stress of the larger particles all over the section of the tube. On the contrary, the streamwise kinetic stress of 60 μm particles decrease in the high shear region only while a slight increase of u_{p60}' is detected in the core flow. The striking result in figure 5 is of course the strong increase of the radial fluctuating velocities of the glass beads for $M_j = 110\%$. Particle-particle collisions should therefore be responsible for an isotropisation of the fluctuating motion of the glass beads among the size classes (kinetic energy transfer) and in each size classes (transfer between components). The main contributor is expected to be the large size class via its fluctuating kinetic energy. A more detailed analysis is presented in the discussion.

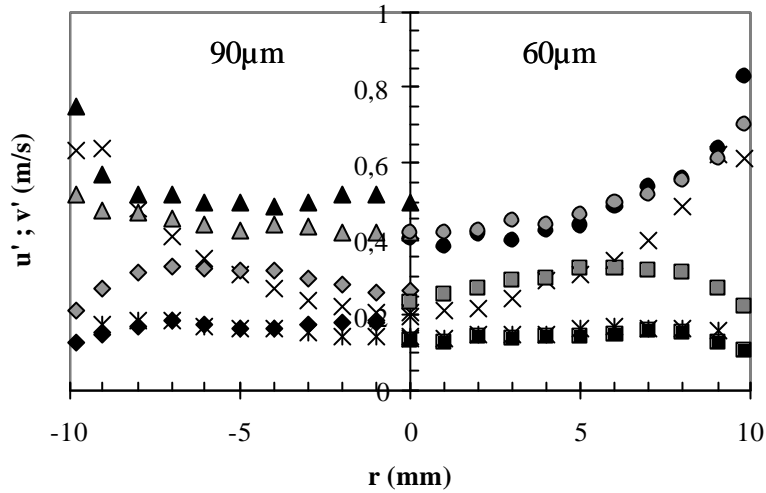


Fig. 5. Longitudinal and radial fluctuating velocity. X, u_f' Tracers; * v_f' Tracers;
 Right side. $d_p = 60\text{mm}$? , u_p' at $M_j = 11\%$; ? , u_p' at $M_j = 110\%$; ! , v_p' at $M_j = 11\%$; ! , v_p' at $M_j = 110\%$;
 Left side. $d_p = 90\text{mm}$? , u_p' at $M_j = 11\%$; ? , u_p' at $M_j = 110\%$; ? , v_p' at $M_j = 11\%$; ? , v_p' at $M_j = 110\%$.

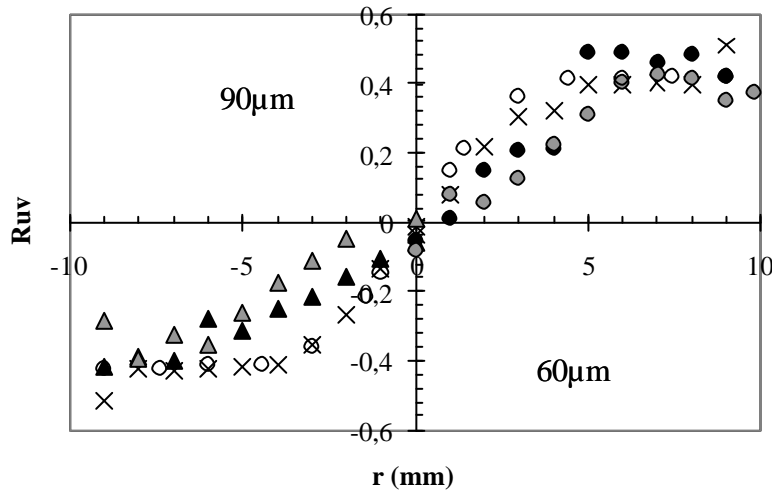


Fig. 6. Profile of the correlation coefficient $R_{uv} = \langle uv \rangle / u'v'$
 X, Tracers; ? , data of (Sabot and Comte-Bellot 1976) ;
 Right side. $d_p = 60\text{mm}$? , $M_j = 11\%$; ? , $M_j = 110\%$;
 Left side. $d_p = 90\text{mm}$? , $M_j = 11\%$; ? , $M_j = 110\%$.

One has to be very careful in interpreting this non-homogeneous flow. The role of collisions is indeed not the same all over the tube because the anisotropy of the fluctuating motions of the glass beads is large in the near wall region only. The radial evolutions of the turbulent transport terms have to be examined before proposing a physical interpretation of these observations at higher loadings.

The turbulent shear stress of the fluid and particulate phase has been displayed in figure 4. The radial turbulent transport of the fluctuating longitudinal momentum of the glass beads by the fluctuating radial velocity is seen to be high, particularly at high mass loading $M_j = 110\%$. The profile of the correlation coefficient (figure 6) $R_{uv} = \langle uv \rangle / u'v'$ of the fluid phase at $M_j = 11\%$ is in good agreement with that of (Sabot and Comte-Bellot 1976) although the Reynolds number of their flow was much higher (respectively $Re_0 = 68000$ and 135000). We observe that a decrease of R_{uv} is measured at the higher mass loading.

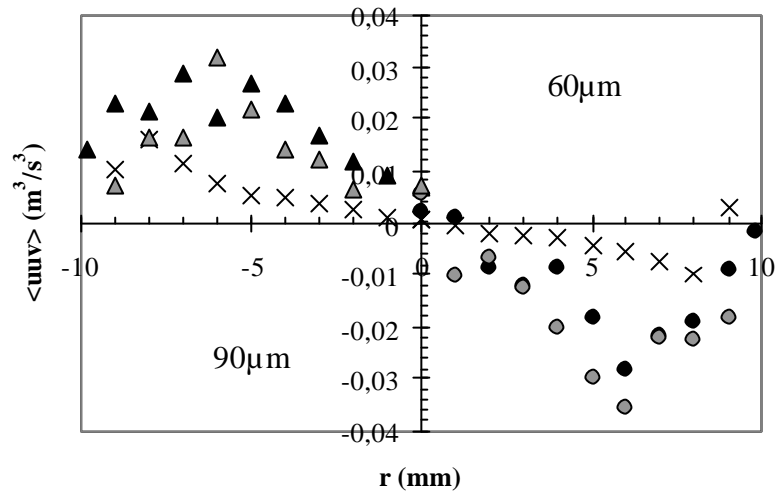


Fig. 7. Radial turbulent transport of longitudinal fluctuating kinetic stress. X, Tracers; Right side. $d_p = 60\mu\text{m}$? , $M_j = 11\%$; ? , $M_j = 110\%$; Left side. $d_p = 90\mu\text{m}$? , $M_j = 11\%$; ? , $M_j = 110\%$.

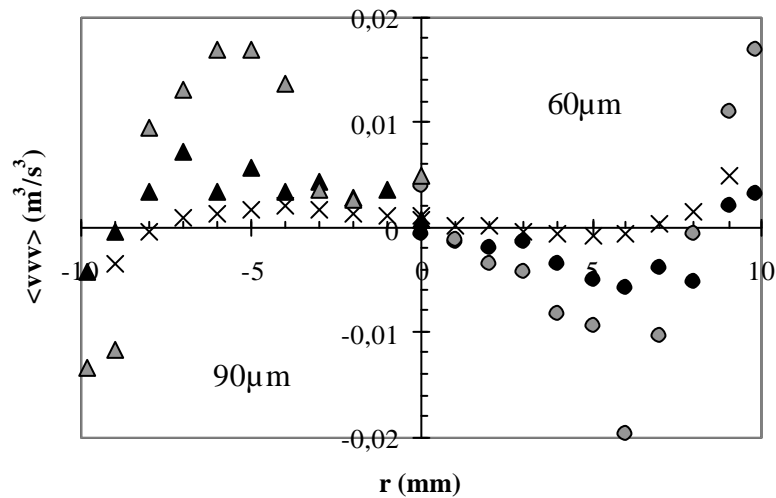


Fig. 8. Radial turbulent transport of radial fluctuating kinetic stress. (Symbols : see fig 7)

The profiles of the third-order moments $\langle uuv \rangle$ and $\langle vvv \rangle$ presented in figure 7 and 8 are more difficult to obtain but reveal very important features of this flow. At both mass loading, the radial turbulent transport of the longitudinal or radial fluctuating kinetic stresses are much larger than the fluid one. This feature was analysed in (Caraman et al. 2003) in relation with a quadrant analysis of the particle velocity statistics in the core region. At low mass loading, this analysis shows that the partly responsive particles, because of their inertia, keep some memory of the lower streamwise velocity existing in the near wall region while they fly across the tube. Again, third order moments in mono and bi-dispersed situations are very similar at low mass loading. The collisions in the near wall region thus partly drive the radial transport of the fluctuating kinetic energy of the particles and have a strong indirect influence on the whole kinetic energy balance.

An increase of the mass loading in the bidispersed situation induces a moderate modification of $\langle uuv \rangle$ with an increase for 60 μm glass beads and a decrease for large 90 μm glass beads. An important evolution of $\langle vvv \rangle$ is observed with a very strong increase of the radial transport of the radial fluctuating kinetic energy. This observation is expected to be associated with the strong increase of v_p' at the higher mass loading (fig. 5).

To insist on that point, we compare in figures 9 and 10 the normalised pdf of the longitudinal and radial fluctuating motions of 60 μm particles at $M_j = 11\%$ and $M_j = 110\%$ and at $r = -6\text{mm}$. The negative dissymmetry of the longitudinal fluctuating motion and the positive dissymmetry of the radial fluctuating motion are very clear. At $r = -6\text{mm}$ (see fig.1), these tails correspond to 60 μm particles flying toward the core region of the tube - positive value of v or v^3 - while keeping the memory of the lower streamwise velocities existing in the surrounding wall region - negative velocities of u or u^3 . We also note that the shape of these normalised pdf is quite similar. However, the probability of finding a positive value of v larger than its rms value $Prob(v_{p60}' \leq v)$ is clearly larger at $M_j = 110\%$ than at $M_j = 11\%$. In the present situation, an increase of the mass loading is thus responsible for a larger value of the transport by the fluctuating motion toward the core of the pipe. This effect is not obvious "a priori" because if collisions were dominant in the core region, they would tend to decrease the particle mean free path (Lavieville 1997) and they would therefore strongly decrease this transport. The present situation is therefore expected to be an intermediate one in which the role of collisions of 60 μm particles with larger partners is moderate in the core flow.

5. DISCUSSION

In a polydispersed particle laden flow, the probability of collision between a particle of size class "i" and the class "j" depends on particle "j" concentration, particles sizes, mean slip motion and fluctuating motion of both classes. Only binary collisions are considered here. The frequency of collisions for class "i" is the sum of the frequency of collisions with each size class $f_{Ci} = \sum_{class} f_{Ci,j}$. The correlation of the velocities of colliding particles is not taken into account in

the present analysis. Results valid in the kinetic theory limit are used (Abrahamson 1975). To take into account both collisions due to fluctuating motion and collisions due to mean drift between particles, $f_{Ci,j}$ can be computed as the sum of two asymptotic situations corresponding respectively to turbulent fluctuations and low mean drift $f_{TCi,j}$ and to high drift $f_{DCi,j}$ (Gourdel et al. 1998) with:

$$f_{Ci,j} = f_{TCi,j} + f_{DCi,j} \quad (5.1)$$

$$f_{TCi,j} = 2^{3/2} \mathbf{p}^{1/2} n_j (r_{pi} + r_{pj})^2 \sqrt{\mathbf{s}_{pi}^2 + \mathbf{s}_{pj}^2} \quad (5.2)$$

$$f_{DCi,j} = \mathbf{p} n_j (r_{pi} + r_{pj})^2 \| \langle \mathbf{U}_p \rangle_{pi} - \langle \mathbf{U}_p \rangle_{pj} \| \quad (5.3)$$

In relations (5.2) and (5.3), r_p is the radius of the particle, n_j is the number concentration for class j deduced from mass concentration measurements and \mathbf{s}_{pi}^2 is the averaged fluctuating component: $\mathbf{s}_{pi}^2 = (u_{pi}^2 + v_{pi}^2 + w_{pi}^2) / 3 \approx (u_{pi}^2 + 2.v_{pi}^2) / 3$. This relation is exact on the axis of the tube flow. More general but also more complex relations are found in (Gourdel, Simonin and Brunier 1999).

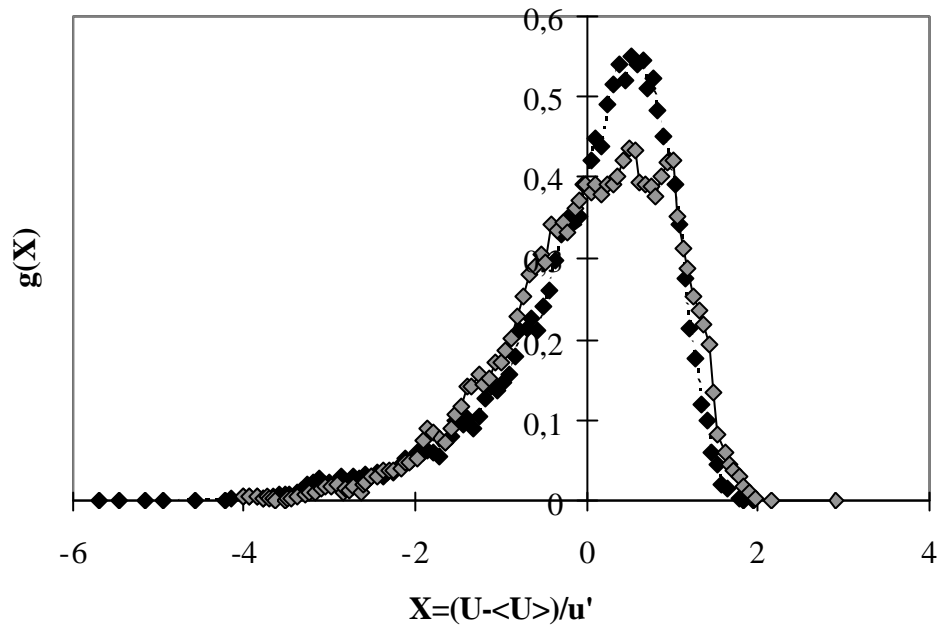


Fig. 9. $d_p = 60\text{mm}$. Normalised probability density functions of the longitudinal motion at $r=-6\text{mm}$.
 $?$, $M_j = 11\%$; $?$, $M_j = 110\%$.

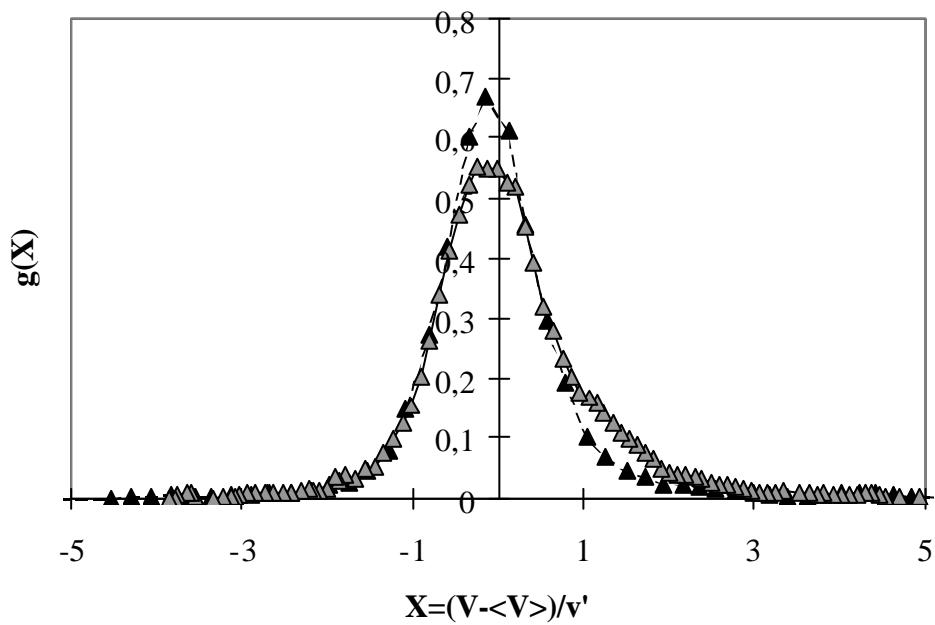


Fig. 10. $d_p = 60\text{mm}$. Normalised probability density functions of the radial motion at $r=-6\text{mm}$.
 $?$, $M_j = 11\%$; $?$, $M_j = 110\%$.

For a monodispersed distribution of glass beads, the collision term contributes to the redistribution of kinetic energy among the various kinetic stresses. For a bidispersed (or polydispersed) distribution, collisions should participate (i) to a transfer of mean momentum between size classes, (ii) to a redistribution of fluctuating kinetic energy between all colliding classes and (iii) to a redistribution of energy between all the fluctuating components. In figure 3, we see that we don't measure any significant reduction of the mean drift velocity between size classes when the mass loading is increased. Obviously, the kinetic stresses are however very sensitive to an increase of mass loading (fig. 5).

The ratio between the averaged time between collisions $t_C = 1/f_C$ and the particle aerodynamic time t_p is a first indicator to evaluate the impact of inter-particle collisions on the fluctuating motion of the dispersed phase. The Stokesian particle relaxation time for $r_p \gg r_f$ is $t_p = r_p d_p^2 / 18\mu$ where d_p is the median diameter of the particle size class and μ is the fluid viscosity. This characteristic time calculation is interesting as a first order of magnitude for particle Reynolds number up to order of unity. The ratio $N_{Ci,j} = t_{Ci,j} / t_{pi}$ is presented respectively in the near wall region ($r=9\text{mm}$ – table 1) and on the axis of the tube ($r=0\text{mm}$ – table 2). Four ratio are computed because we separate inter-class and in-class contributions. Note that the mean drift effect (eq. 5.3) is negligible on the tube axis but accounts for about 25% of the mean inter-class collision frequency at $r=9\text{mm}$.

$r = 9\text{mm}$	$t_{C60,90}/t_{p60}$	$t_{C60,60}/t_{p60}$	$t_{C90,90}/t_{p90}$	$t_{C90,60}/t_{p90}$
$M_j = 11\%$	16.2	60.4	6.9	13.4
$M_j = 110\%$	1.6	5.8	0.7	1.4

Table. 1. Ratio between the averaged time between collisions and the particle aerodynamic time at $r=9\text{mm}$.

Axis	$t_{C60,90}/t_{p60}$	$t_{C60,60}/t_{p60}$	$t_{C90,90}/t_{p90}$	$t_{C90,60}/t_{p90}$
$M_j = 11\%$	22.0	90.2	7.2	18.4
$M_j = 110\%$	2.4	7.8	0.8	2.0

Table.2. Ratio between the averaged time between collisions and the particle aerodynamic time at $r=0\text{mm}$.

Tables 1 and 2 first show that N_C is very large at the lowest mass loading $M_j = 11\%$. The radial evolution of the mean and fluctuating velocity of $60\mu\text{m}$ particles are noticeably very similar in monodispersed (Caraman et al. 2003) or bidispersed situations at this low mass loading. The same physical mechanisms are therefore expected to drive the fluctuating motion of the $60\mu\text{m}$ glass beads in this case. Particle-particle collisions provide a very important direct contribution to v_p' in the near wall region only. There the turbulence entrainment is negligible and the dominant effects concerning the wall-normal velocity variance are a production through the collision redistribution mechanism from the very large streamwise velocity variance to the radial velocity variance, a dissipation due to the fluid drag and a transport by the third order velocity correlation. In the core of the flow, the redistribution effect through collisions becomes negligible due to the much smaller values of the streamwise velocity variance and the dominant effects are a production through the interaction with the fluid turbulence, a dissipation due to the drag force and a transport by the third order velocity correlation (from the near wall regions).

Collisions are more probable at the higher mass loading. Using the work of (Gourdel 1999), it is possible to show that the redistribution of fluctuating kinetic energy between $60\mu\text{m}$ and $90\mu\text{m}$ glass beads is a significant term. The consequences are clearly observed in figure 5 where we see that both longitudinal and radial kinetic stresses of $60\mu\text{m}$ and $90\mu\text{m}$ size classes are very similar at $M_j = 110\%$. The precise evaluation of the redistribution between fluctuating components is difficult to perform. However, the anisotropy of the fluctuating motion is still large in the near wall region and the

probability of collision increases significantly at $M_j = 110\%$. We therefore expect an important contribution of inter-particle collisions to the radial variance v_p' in the near wall region associated to a damping of the longitudinal kinetic stress. This damping is more important for $90\mu\text{m}$ glass beads than for $60\mu\text{m}$ glass beads because $60\mu\text{m}$ particles receive kinetic energy from $90\mu\text{m}$ particles. In the core region, it is important to note that collisions are significant but not dominant with $N_{C60} \approx 2$ and $N_{C90} \approx 1$. The non-dimensional radial distance covered by a glass bead at the radial rms velocity and during its time scale is $v_{p60}' \cdot t_{p60} / D_0 \approx 0.34$ and $v_{p90}' \cdot t_{p90} / D_0 \approx 0.8$. Particles, because of their inertia, can thus keep the memory of the lower streamwise velocities and higher radial velocities while they fly over the tube and interact with the core turbulence. This explain why transport effects of both longitudinal and radial fluctuating kinetic stresses are very high (see fig. 7 and 8) and why normalised pdf are quite similar at $M_j = 110\%$ and $M_j = 11\%$ (see fig. 9 and 10). For a stronger increase in mass loading, leading to $N_{C60} \ll 1$ and to dominant effects of collisions, one would expect these transport terms to be of minor importance. Measurements would unfortunately be very difficult in these situations.

6. CONCLUSION

The present paper was devoted to the measurement and analysis of a bidispersed two-phase flow at low (11%) and moderate (110%) mass loading in a fully developed pipe flow. Our goal was to provide data and analysis showing unambiguously the role of inter-class collisions. The mass distribution of the mixture of particles was therefore chosen in order to promote the collisions of the large $90\mu\text{m}$ particles with $60\mu\text{m}$ glass beads.

Velocity statistical moments up to the third order moments and at both mass loadings were presented and discussed. At low mass loading, it is interesting to note that the radial characteristics of the air and $60\mu\text{m}$ glass beads for a monodispersed (Caraman et al. 2003) and a bidispersed situations (present results) are very similar. Note that the radial turbulent transport of longitudinal and radial fluctuating kinetic stresses is much higher for the particles than for the fluid phase. Dominant effects in the flow are then (i) in the core flow a source through the interaction with the fluid turbulence, a dissipation due to the fluid drag and a transport by the third order velocity correlation.; (ii) in the near wall region a production by the mean shear for u_p' and a redistribution from the very large streamwise velocity variance via particle-particle collisions for v_p' .

The signature of inter-particle collisions is very clear at higher mass loading. In particular, we measure a decrease of the streamwise kinetic stress of the larger particles all over the section of the tube. On the contrary, the streamwise kinetic stress of $60\mu\text{m}$ particles decrease in the high shear region only while a slight increase of u_{p60}' is detected in the core flow. The striking result is the strong increase of the radial fluctuating velocities of the glass beads and of the radial transport of the radial fluctuating kinetic energy for $M_j = 110\%$.

An analysis of the collision frequency in different regions of the flow shows that, even at $M_j = 110\%$, the mean time scale between collisions is of the order or larger than the particle aerodynamic time constant. The picture at the higher mass loading studied here is thus an important contribution of inter-particle collisions to the radial variance v_p' in the near wall region associated to a damping of the longitudinal kinetic stress. This damping is more important for $90\mu\text{m}$ glass beads than for $60\mu\text{m}$ glass beads because $60\mu\text{m}$ particles receive kinetic energy from $90\mu\text{m}$ particles. However, collisions are not able to decrease significantly the mean free path of the particle fluctuating motion. Therefore, transport effects of both longitudinal and radial fluctuating kinetic stresses toward the core region are very high while normalised pdf are quite similar at $M_j = 110\%$ and $M_j = 11\%$.

The present study shows that accurate models describing the full particle kinetic stresses and the exchanges due to the collisional terms are very important for the accurate prediction of gas-solid polydispersed tube flows. A further study of the role of inter-particle collisions on turbulent transport terms in non-homogeneous situations would be important to understand the transition from negligible to dominant collision effects in the core flow.

ACKNOWLEDGEMENTS

We thank Dr T. Ishima for his participation in the early part of this research. We thank J.D. Mattei, of the research department M.F.T.T. of EdF - R&D who accepted to keep on the long way necessary to obtain reliable experimental results. The technical support of P. Fanouillère is greatly acknowledged.

REFERENCES

- Abrahamson, J. (1975). Collision rates of small particles in a vigorously turbulent fluid. *Chem. Eng. Sci.* **30**: 1371-1379.
- Benedict, L. H. and Gould, R. D. (1996). Uncertainty estimates for any turbulence statistics. Eighth International Symposium on applications of Laser techniques to Fluid Mechanics, Lisbon.
- Borée, J., Ishima, T. and Flour, I. (2001). The effect of mass loading and inter-particle collisions on the development of the polydispersed two-phase flow downstream a confined bluff body. *J. Fluid Mech.* **443**: 129 - 165.
- Caraman, N., Borée, J. and Simonin, O. (2003). Effect of collisions on the dispersed phase turbulence in a dilute tube flow. Experimental and Theoretical analysis. *Physics of Fluids* **15**, (12).
- Gourdel, C. (1999). Modélisation et simulations de mélanges binaires de particules en interaction avec un champ fluide turbulent pour l'application aux lits fluidisés circulant, U.T.C.
- Gourdel, C., Simonin, O. and Brunier, E. (1998). Modelling and simulation of gas-solid turbulent flows with a binary mixture of particles. Third International Conference on Multiphase Flows, ICMF'98, Lyon, June 8-12.
- Gourdel, C., Simonin, O. and Brunier, E. (1999). Two-Maxwellian equilibrium distribution function for the modelling of a binary mixture of particles. Circulating Fluidized Bed Technology VI, Frankfurt am Main, Germany.
- Kussin, J. and Sommerfeld, M. (2002). Experimental studies on particle behaviour and turbulence modification in horizontal channel flow with different wall roughness. *Exp. in Fluids* **33**: 143-159.
- Lavieville, J. (1997). Simulation numérique et modélisation des interactions entre l'entraînement par la turbulence et les collisions interparticulaires en écoulements gaz-solides. Thèse de l'université de Rouen.
- Sabot, J. and Comte-Bellot, G. (1976). Intermittency of coherent structures in the core region of fully developed turbulent pipe flow. *J. Fluid Mech.* **74**: 767-796.
- Simonin, O., Wang, Q. and Squire, K. D. (1997). Comparison between Two-Fluid model predictions and large eddy simulation results in a vertical gas-solid turbulent channel flow. Proc. 7th int. Symp. on Gas-particle flows, ASME. FEDSM'97-3625.
- Sommerfeld, M. (2003). Analysis of collision effects for turbulent gas-particle flow in a horizontal channel: Part I. Particle transport. *Int. J. Multiphase Flow* **29**: 675-699.
- Yamamoto, Y., Potthoff, M., Tanaka, T., Kajishima, T. and Tsuji, Y. (2001). Large-eddy simulation of turbulent gas-particle flow in a vertical channel: effect of considering inter-particle collisions. *J. Fluid Mech.* **442**: 303-334.